

Thermoplastic starch and poly(ϵ -caprolactone) blends: morphology and mechanical properties as a function of relative humidity

A. Mahieu · C. Terrié · A. Agoulon · N. Leblanc · B. Youssef

Received: 12 April 2013 / Accepted: 17 July 2013 / Published online: 9 August 2013
© Springer Science+Business Media Dordrecht 2013

Abstract This paper describes the elaboration and characterization of biodegradable films from thermoplastic starch (TPS) and poly(ϵ -caprolactone) (PCL) blends. The films were obtained by a single screw extrusion process. Two PCLs of different molecular weights (37,000 and 50,000 g.mol⁻¹, referred as PCL37 and PCL50) have been tested. Phase distribution of PCL and thermoplastic starch (TPS) has been characterized by FTIR, DSC and SEM. For the blend with PCL37, material surface is enriched with PCL, whereas in the blend with PCL50, TPS and PCL phases are more homogeneously distributed. Evolution of crystalline structure of the different formulations has been studied by X-ray diffraction, and mechanical properties by tensile tests. Maximal deformation of TPS/PCL blends is smaller than that of TPS, attesting the lack of compatibility between both polymers. Blending with PCL modifies the crystalline structure of TPS. Water resistance of the blends has been characterized by water sorption and water contact angle measurements. The decrease in water absorption for the blends was attributed to the decrease of starch content. At the surface of the material, water resistance of TPS/PCL50 blends is improved.

Keywords Poly(ϵ -caprolactone) · Starch · Blends · Mechanical properties · Relative humidity

A. Mahieu · C. Terrié (✉) · N. Leblanc
Unité de recherche AGRI'TERR - équipe LGMA, Esitpa,
3 rue du Tronquet, 76 134 Mont Saint Aignan Cedex, France
e-mail: cterrie@esitpa.org

A. Mahieu · B. Youssef (✉)
AMME - LECAP, EA4528, International Laboratory,
Institut des Matériaux de Rouen, Université et INSA de Rouen,
BP12, 76801 Saint Etienne du Rouvray Cedex, France
e-mail: boulos.youssef@univ-rouen.fr

A. Agoulon
AGRO-HALL, 55 rue Saint Germain, 27000 Evreux, France

Introduction

Concern for the environment over the past decades has led to extensive work aimed at replacing petrochemical-based plastic materials by renewable polymers. In this field, starch has attracted considerable attention due to its natural abundance, and its ability to transform into thermoplastic resin-like products under destructuring and plasticizing conditions [1–3]. Starch is a polysaccharide extracted from a variety of plants such as corn, wheat, rice or potatoes. The two major macromolecules composing starch are amylose, a linear polymer consisting of α -1,4 linked D-glucose units, and amylopectin, a highly branched structure of short α -1,4 chains linked by α -1,6 bonds. Thermoplastic starch (TPS) has several advantages such as total compostability and renewability of the resource [1]. Besides, it can be easily processed with conventional plastic processing machines [4], and shows a wide range of properties according to the plasticizer level and the starch botanical source [5]. One interesting property for packaging application is that TPS oxygen permeability is found low compared with most polyesters [6]. The best gas barrier properties of starch based films are generally obtained for low water and plasticiser contents [7]. However, TPS is a very hydrophilic material with limited performances for some applications. Its major drawbacks are its water sensibility and low mechanical properties: TPS water permeability is high due to its polar character, mechanical properties decrease and gas permeabilities increase in high humidity environments [8]. To overcome these issues while maintaining its biodegradability, one strategy consists in associating TPS with another biodegradable polymer [9]. Blends of TPS with several synthetic biodegradable polymers have been investigated in the literature: poly(lactic acid) (PLA) [10], poly(vinyl alcohol) (PVOH) [11, 12], poly(ethylene oxide) (PEO) [13], polybutylene succinate adipate (PBSA) [14]... Among them, polycaprolactone (PCL)/TPS blends can be an interesting way of improving

mechanical and water and oxygen barrier properties of starch based films [15].

Poly(ϵ -caprolactone) (PCL) is a linear, hydrophobic and partially crystalline polyester. Its physical properties and commercial availability make it very attractive, not only as a substitute of non-biodegradable polymers for convenience products, but also for specific applications in the medical and agricultural fields [16–18]. For instance, starch/PCL blends have been studied for biomedical applications such as tissue engineering [19]. TPS and PCL are usually considered as non-miscible polymers [20, 21]. During the extrusion of plasticized starch/polycaprolactone blends, a phase separation phenomenon occurs. In certain conditions, a pseudo-multilayer structure can be generated with a polyester rich skin. It was shown that this phase separation is mainly driven by the molecular weight of polycaprolactone, linked to its molten state viscosity [21]. On the other hand, according to Li [4], TPS and PCL have been found to be miscible when TPS contains a high plasticizer rate and under appropriate extrusion parameters. This author pointed out a strong tendency of polycaprolactone to encapsulate the thermoplastic starch, property which could also lead to the improvement of TPS water resistance by blending with PCL.

In this work, we describe the elaboration and characterization of biodegradable films from thermoplastic starch (TPS). Our aim was to improve the properties of TPS films by blending with polycaprolactone (PCL). For this reason, several materials were prepared with 2 PCLs differing in molar mass (37 000 or 50 000 $\text{g}\cdot\text{mol}^{-1}$) and by processing at varying extrusion screw speeds. The morphology of the blends was studied to estimate the phase repartition between TPS and PCL. Mechanical and water properties were investigated to evaluate the effect of this phase repartition on the properties of the material, at different relative humidities.

Experimental

Materials

Unmodified wheat starch and glycerol were obtained from Sigma Aldrich (France). Wheat starch contains 26 % amylose ($M_w \sim 1.5 \cdot 10^6 \text{ g}\cdot\text{mol}^{-1}$ [22]) and 74 % amylopectin. M_w of amylopectin was estimated around $1.10^9 \text{ g}\cdot\text{mol}^{-1}$ [23].

PCL CAPA 6,400 and 6,500 were purchased from Perstorp (UK). Their average molecular weights are respectively 37 000 and 50 000 $\text{g}\cdot\text{mol}^{-1}$ (referred respectively as “PCL37” and “PCL50”).

Sample preparation

TPS compounds were prepared by extruding native wheat starch with 20 % glycerol, which has been shown to be the

maximum rate leading to starch plasticization without phase separation between starch and glycerol [24, 25]. Components were previously blended in a thermo-regulated turbo-mixer and heated in an oven at 170 °C for 1 h, allowing diffusion of glycerol into the starch granules. Then water was added to adjust the humidity rate of this blend at 10 % w/w. In a first step, the obtained powder was extruded and granulated in a single screw extruder (SCAMEX, France) equipped with three heating zones regulated at 100 °C, then 110 °C around the screw and 90 °C for the die.

In a second step, these TPS compounds were blended with 30 % w/w PCL37 or PCL50, then extruded and granulated in the same conditions as in the first step. The final step consisted in extruding these blended compounds through a slit die to obtain films (about 1 mm thickness). Temperatures used on the extruder were 110 °C, 120 °C and 100 °C, at various screw speeds in the range 10–70 rpm.

Pure starch films were produced by extruding plasticized starch compounds obtained after the first step at 120 °C through the slit die. Commercial PCL granules were extruded at 80 °C through the slit die and then calendered to give pure PCL films. Rheological measurements during extrusion could be performed using a rheological die (SCAMEX) instead of the slit die.

Films were stored in controlled chambers at different relative humidities (RH): 33 %, 53 % and 75 % RH, using saturated salt solutions with respectively MgCl_2 , $\text{Mg}(\text{NO}_3)_2$ and NaCl [26].

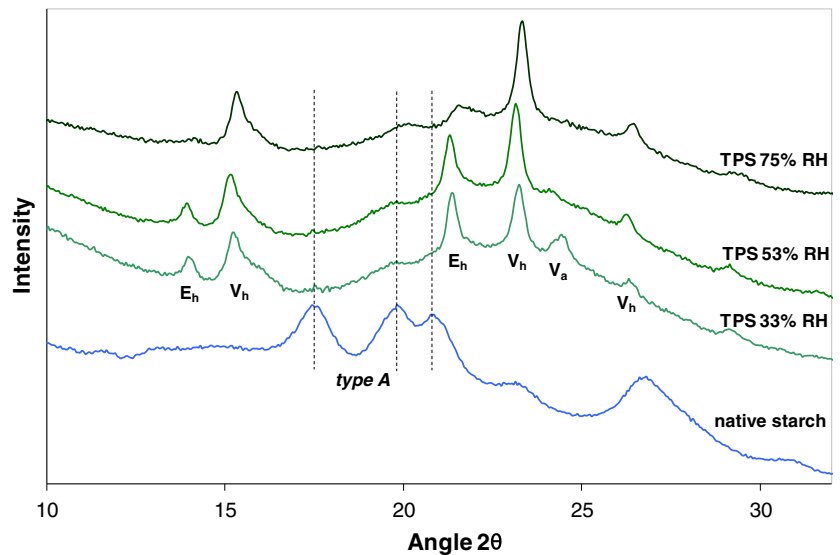
Thermal analysis (DSC)

Calorimetric measurements were conducted on a temperature modulated differential scanning calorimeter (TA Instrument Q100). Samples of approximately 10 mg (about 50 μm thickness) were cut separately on the film surface or on the film core (500 μm from the surface) and placed in a hermetic aluminium pan. The sealed pans including samples were weighed before and after the measurement to check the absence of water evaporation. Two successive scans of each sample were performed from -90 °C to 120 °C with a heating rate of 10°/min. The thermal effects were studied on the thermogram obtained during the second heating run to suppress any possible difference in thermal history between the samples. Calibrations in temperature and energy were done by measuring the temperature and the enthalpy of melting of Indium.

Fourier transformed infrared spectroscopy (FTIR)

The FTIR spectra were recorded on a Nicolet iS10 spectrophotometer (Thermo scientific) equipped with a diamond crystal in attenuated total-reflectance mode (ATR). A series of 64 scans were collected for each measure over the 4,000 to 650 cm^{-1} spectral range with a 4 cm^{-1} resolution. Spectra were

Fig. 1 XRD patterns for native starch and pure TPS (50 rpm) at different relative humidities



analyzed with the Omnic 8.1 software. Measurements are performed separately on the film surface or on the film core. Series of six experiments were carried out on each sample.

Wide angle X-ray diffraction

The structures of the samples were tested with X-ray diffraction experiments using a Bruker D8 Advance wide angle X-ray diffractometer. X-ray diffraction patterns were performed on a sample of the entire film after conditioning in a controlled humidity atmosphere. Experiments were carried out with Co K α radiations ($\lambda=1.78897 \text{ \AA}$), the scattering angle (2θ) covered the range from 10° to 35° (θ is the Bragg angle) with a step of 0.05° and a sampling interval of 0.5 s. Measurement cycles are repeated during 3 to 4 h to obtain a smooth curve.

Sorption measurements

Vapour water sorption-isotherms of each sample were deduced from the static-gravimetric technique of water vapour-sorption by using saturated salt-solutions at 23°C . These solutions were prepared to generate an environment with controlled humidity in a closed chamber. Square samples of 2 cm^2 of each material were cut and dried in a desiccator under vacuum and in presence of P_2O_5 . Then samples were placed in triplicate in chambers with different relative humidity obtained with above-saturated salt solutions of LiBr (6 % RH), LiCl (11 % RH), CH_3COOK (23 % RH), MgCl_2 (33 % RH), $\text{Mg}(\text{NO}_3)_2$ (53 % RH), CoCl_2 (65 % RH), NaCl (75 % RH), KCl (85 % RH) and KNO_3 (94 % RH) respectively [26]. Samples were weighted until equilibrium for

Fig. 2 X-ray diffractograms of pure PCL, pure TPS and TPS/PCL blends processed at different screw speeds (53 % RH)

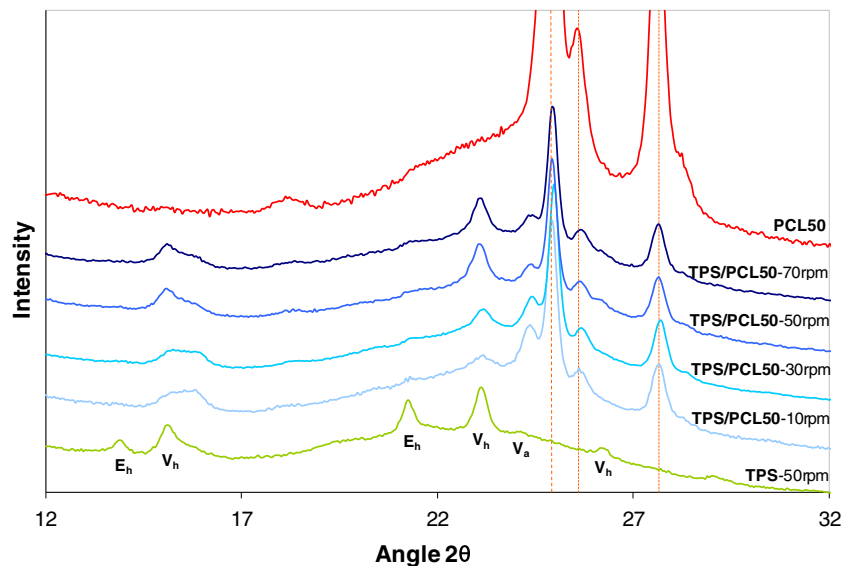


Table 1 Extrusion flow rates for TPS and TPS/PCL50 at various screw speeds

Extrusion screw speed (rpm)	Extrusion flow rate (g.min ⁻¹)	
	TPS	TPS/PCL50
10	4.4±0.3	11.7±0.8
30	17±1	35±2
50	31±4	61±2
70	48±4	75±4

1 month. Water sorption isotherms were obtained by plotting maximal water content of the material as a function of water activity.

Water sorption isotherms were fitted according to Park's model [27], which has been found suitable for the description of the sorption behaviour of cellulosic [28] and starch-based materials [29]. This model assumes the association of three mechanisms: non-specific sorption (Henry's law), specific sorption (Langmuir's mode), and water molecules aggregation at high water activity [28]. In this model, the equilibrium moisture content M as a function of water activity a_w is given by:

$$M = \frac{A_L \cdot b_L \cdot a_w}{1 + b_L \cdot a_w} + k_H \cdot a_w + K_a \cdot a_w^n \quad (1)$$

with A_L the Langmuir capacity constant (concentration of specific sorption sites), b_L the Langmuir affinity constant of water for these sites, k_H the Henry's solubility coefficient, K_a

the equilibrium constant of water aggregation and n the mean number of water molecules per cluster.

To evaluate the accuracy of Park's model to describe the experimental water sorption isotherms of our materials, the mean relative percentage deviation modulus (E) was used; with a value below 10 % revealing a good fit [30].

Contact angle measurements

The surface tension of the materials was calculated according to the Owens-Wendt method [31], using contact angle measurements. Three reference liquids were used: ultra pure water (milli-Q Water System, resistivity 18 $\Omega \cdot \text{cm}^{-1}$), glycerol and diiodomethane. All measurements were carried out at room temperature (23 °C). A drop of 3 μL was deposited with a micro syringe on the surface of a small sample cut in the centre of each film. The drop was recorded by a video camera and an image analysis software (Wingoutte) was used to determine the contact angle. Each presented value is an average of six droplets on the same sample, that is to say 12 angle values (angles measured on left and right side of the drop).

To study the absorption of water at the surface of the materials, the evolution of a water droplet shape was recorded by a video camera. Contact angle θ_i was measured as previously described, as a function of time. Results are given as the relative variation of the measured angle θ_i compared to the initial angle (θ_{max}).

Surface roughness measurements

The surface roughness of the films were determined using a Perthometer M1 (Mahr, France) apparatus. The roughness

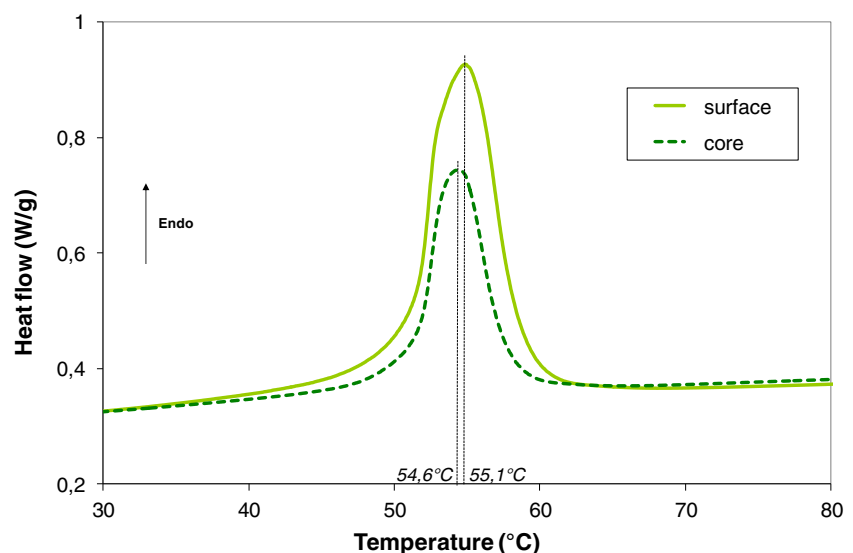
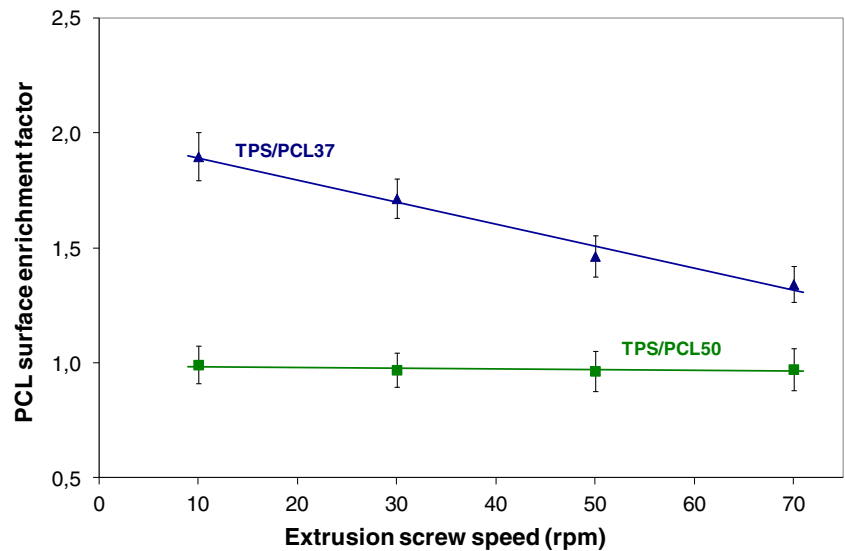
Fig. 3 Thermograms of the surface and the core of the film TPS/PCL37 extruded at 10 rpm

Fig. 4 PCL enrichment factor measured by DSC as a function of extrusion screw speed



representative value measured is the arithmetic mean value R_a . It corresponds to the arithmetic average on a basis length l (5.6 mm) of all the distances y between the average line and the profile:

$$R_a = \frac{1}{l} \int_0^l |y(x)| \cdot dx \quad (2)$$

The given values were calculated as the average of ten measurements of R_a on different zones on the surface of each film.

Mechanical properties

Tensile tests were carried out by using a universal testing machine (Instron model 3365, France). The tests were performed using a load cell of 1 kN at a speed of $5 \text{ mm} \cdot \text{min}^{-1}$ following the international standard ASTM D638. Average values of ten different standard dumbbell specimens were reported.

The samples have been taken in the centre of extruded film and in the extrusion drawn direction. The samples geometry is a standard traction specimen [32]. Prior to analysis, the samples were conditioned under controlled humidity, and the tests were performed at room temperature and humidity, under

Fig. 5 FTIR spectra of TPS film, PCL37 film and the blend TPS/PCL37 carried out separately on the surface and on the core of the film

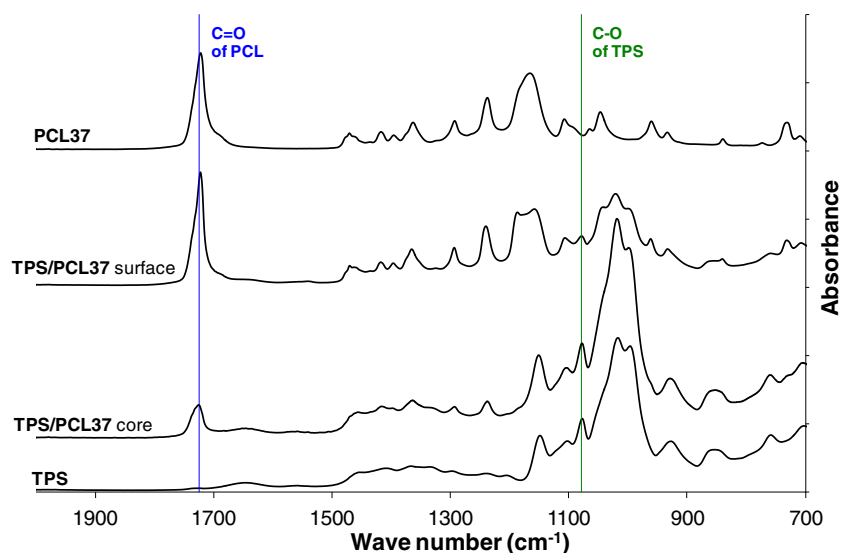
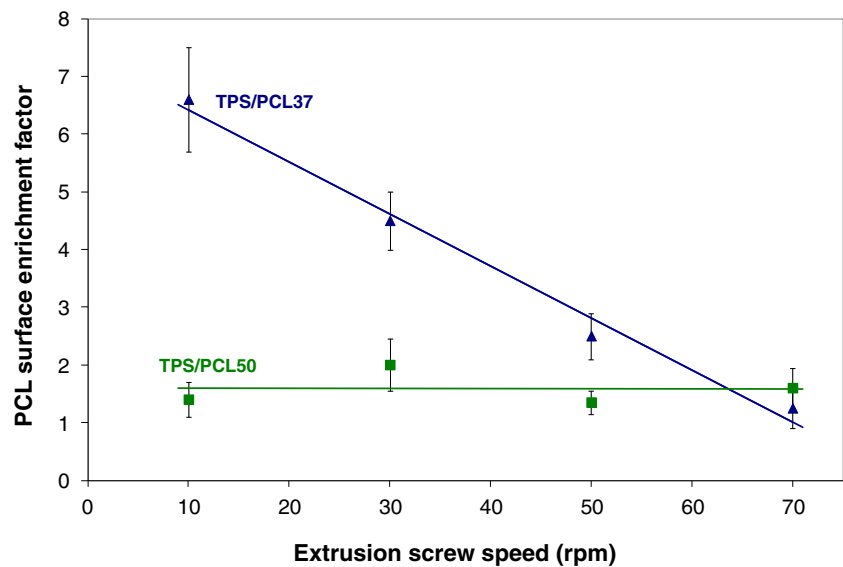


Fig. 6 PCL enrichment factor measured by FTIR as a function of extrusion screw speed

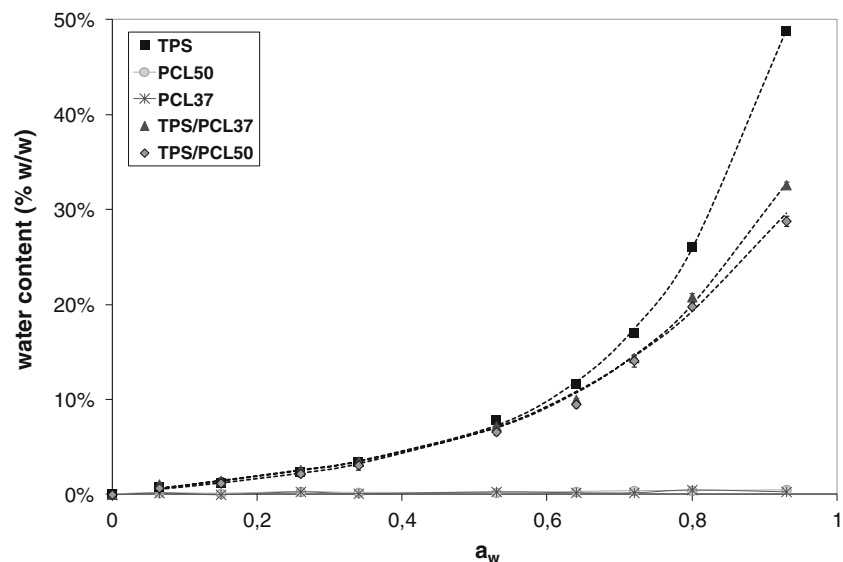


atmospheric pressure. Data were collected with Instron BlueHill 2 software.

Scanning electron microscopy (SEM)

Samples were treated in dichloromethane by Soxhlet extraction experiment during 24 h to solubilise the PCL phase. The amount of remaining PCL after extraction was measured by thermogravimetric analysis (TG 209 F1, Netzsch) and represented 1/3 of the initial amount. After liquid nitrogen freeze-fracture, the exposed surfaces were gold-coated to avoid charging under the electron beam. Film cross sections were observed with a scanning electron microscope (Hitachi, Japan).

Fig. 7 Equilibrium moisture content of TPS/PCL blends at different water activities: experimental points and simulated curves (—) calculated from Park's model



Results and discussion

Crystalline structure

Crystalline structures of starch have been described in the literature [33–36]. Three crystalline structures are observed in native granular starch: double-helical A-, B-, and C-type. During processing of TPS single helical structures can form: V_H -, V_A - or E_H -type structures differing in helix packing [33–36]. Amount and type of crystalline structure is influenced by processing parameters and composition of the material.

X-ray diffraction patterns for native starch and pure TPS at different relative humidities (RH) are presented in Fig. 1. For

Table 2 Parameters of Park model determined from water sorption isotherms for TPS and TPC/PCL blends

	A_L	b_L	k_H	K_a	n_a	E (%)
TPS	0,009	0,42	0,097	0,111	5,3	6,8
TPS/PCL37	0,011	0,59	0,086	0,077	4,3	7,8
TPS/PCL50	0,005	0,70	0,072	0,083	3,6	7,0

native starch, the diffraction peaks are obtained for 2θ values equal to 17.6° , 19.9° , 20.3° , 23.3° and 26.8° , implying that these raw materials present an A-type structure. The absence of A-type characteristic peaks in TPS confirms the deconstruction of native starch granules after extrusion.

At 75 % RH, the 2θ values of diffraction peaks of TPS (15.3° , 23.3° , 26.5°) are characteristic of a V_H crystalline type structure [33]. At lower RH, V_A (24.4°) and E_H (14.0° , 21.3°) structures appear. These experiments show that the crystalline structure of TPS evolves with relative humidity.

Figure 2 displays the XRD patterns of TPS, PCL50 and TPS/PCL50 blends at different extrusion speeds and at 53 % RH. Similar results were obtained with PCL37. Peaks for pure PCL (24.9° , 25.7° , 27.6°) are in agreement with the reported unit cell parameters of PCL [37] and no evolution was noticed whatever the screw speed or RH.

The crystalline structure of TPS in TPS/PCL blends is different from the crystalline structure in pure TPS under the same RH (53 %). In blends, the characteristic peak of V_A (24.4°) structure is present; as for pure TPS stored at 33 % RH; while it is not noticeable when pure TPS is stored at 53 % RH. This suggests that blending with PCL modifies the crystalline structure of starch, which becomes close to a less hydrated

pure starch. PCL thus seems to affect starch/water interactions in the TPS crystalline phase.

For TPS and TPS-PCL50 processed at the same screw speed (50 rpm); the flow rate is higher for the blend (Table 1). Flow rate is inversely proportional to the mean residence time in the extruder [38]; the mean residence time is thus higher for TPS than for TPS/PCL. This could explain the absence of E_H structure in TPS/PCL blends; which was shown to increase with residence time [36].

The crystalline structure of starch in the blends changes when screw speeds decreases: V_H decreases and V_A increases. Lower screw speeds correspond to lower flow rate in the extruder (Table 1), and then to higher mean residence time in the extruder. Since V_A is a less hydrated structure, the humidity in the melted blend during extrusion probably becomes lower when the residence time is longer. This leads to different crystalline structures; remaining afterwards when the materials are equilibrated at 53 % RH.

TPS/PCL phases distribution

DSC analyses were performed at the surface and at the core of the films to investigate the formation of a PCL-rich surface in the TPS/PCL films. In the temperature range 30°C – 80°C , the melting peak observed corresponds to the fusion of the PCL crystalline phase. Figure 3 displays the DSC curves obtained for the TPS/PCL37 blend extruded at 10 rpm, for the surface and the core of the film. A small decrease in melt temperature is observed, compared to pure PCL ($T_m = 57.4^\circ\text{C}$). This effect is more noticeable in the core (54.6°C) than at the surface of the material (55.1°C). This could indicate that a phase separation has occurred; but the slight depression in the melt

Fig. 8 Moisture sorption isotherms related to the starch fraction

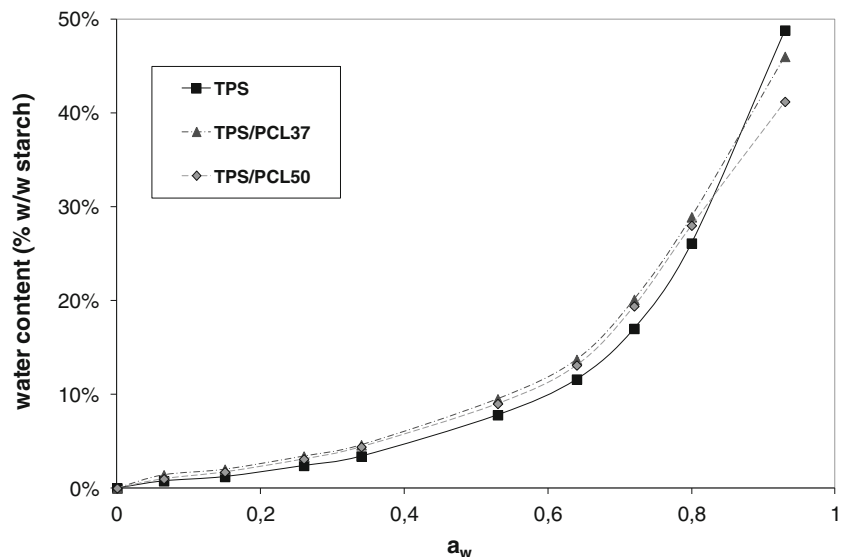


Table 3 Surface tension and initial water contact angle of TPS, PCL and TPS/PCL blends

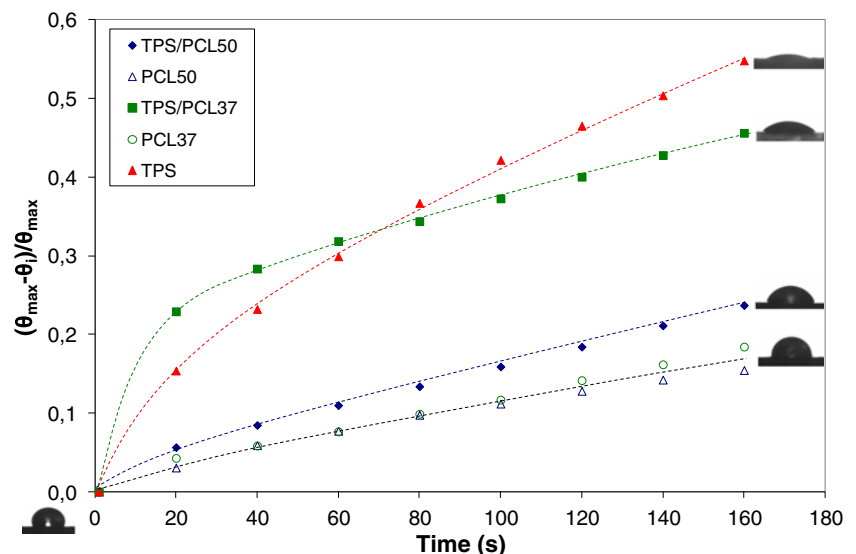
Sample	Surface tension γ (mJ/m ²)	Initial water contact angle θ_{\max}
PCL37	45,6	74.2°
PCL50	44,9	82.0°
TPS	34,8	53.0°
TPS/PCL37	41,5	67.2°
TPS/PCL50	36,1	83.4°

temperature can also be explained by the formation of hydrogen bonds between the hydroxyls of starch and carbonyl of PCL at the interface region and their effect on PCL crystallites, and/or interactions between PCL and TPS plasticizer [39].

A PCL surface enrichment factor was calculated from the ratio of the PCL melting enthalpy at the surface to the PCL melting enthalpy at the core according to the following equation:

$$\text{PCL surface enrichment factor by DSC} = \frac{\Delta H_{m_{\text{surface}}}}{\Delta H_{m_{\text{core}}}} \quad (3)$$

where ΔH_m is the surface under the PCL melting peak, and is proportional to the ratio of crystalline PCL in the sample. This PCL enrichment factor is thus strictly a crystalline PCL surface enrichment factor; however it seems reasonable to use it as the whole PCL enrichment factor. This supposes that PCL crystallinity is the same at the core and at the surface, even if the cooling rate may differ. This assessment is supported by the work of Wang et al. [39] showing that for PCL and starch/PCL blends, crystallinity of PCL is insensitive to cooling rate, at least in their studied range (2.5–40 °C.min⁻¹). Moreover, ΔH_m was measured during the second DSC heat run to suppress any discrepancy between the thermal histories of the samples.

Fig. 9 Relative variation of water contact angle as a function of time for PCL, TPS and TPS/PCL blends (10 rpm) and corresponding pictures of the water drops

Similar experiments were carried out for TPS/PCL37 and TPS/PCL50 blends, both extruded at various screw speeds (10, 30, 50 and 70 rpm). The results are presented in Fig. 4. There is no surface enrichment for PCL 50 whatever the extrusion screw speed. For TPS/PCL37 blends, a PCL surface enrichment is evidenced; it increases when screw speed decreases.

The factor governing the surface enrichment behaviour is the molecular weight, and so the viscosity of the dispersed phase (PCL). Processing conditions can also play a role on the phase separation phenomenon [21]. For PCL50, the viscosity is high (1,500 Pa.s at 30 rpm) and PCL chains are not enough mobile to allow a significant migration towards the surface of the material. On the contrary for PCL37, displaying a lower apparent viscosity during extrusion (260 Pa.s at 30 rpm), PCL mobility is high enough to allow phase separation. The migration of PCL37 chains towards the surface of the material is favoured when the residence time in the extruder is longer; hence at lower screw speeds.

The PCL repartition in the blends was also investigated by FTIR spectroscopy. Examples of the spectra obtained on our films are presented on Fig. 5. The peak at 1,730 cm⁻¹ corresponds to C=O bonds characteristic of PCL. The peak at 1,078 cm⁻¹ is characteristic of TPS phase in the film, corresponding to C-O bonds of starch C-O-H groups.

The enrichment factor in PCL on film surface obtained by FTIR is estimated according to the equation [21]:

$$\text{PCL surface enrichment factor by FTIR} = \frac{\left(\frac{H_{\text{PCLpeak}}}{H_{\text{TPSpeak}}}\right)_{\text{surface}}}{\left(\frac{H_{\text{PCLpeak}}}{H_{\text{TPSpeak}}}\right)_{\text{core}}} \quad (4)$$

where H is the height of the characteristic peaks of TPS or PCL.

The results are presented in Fig. 6. They confirm that PCL surface enrichment is very low with PCL50, whereas there is a

Table 4 Surface roughness of the samples

Sample	Screw speed (rpm)	R _a (μm)
TPS	50	1.4±0.1
PCL	/	0.2±0.1
TPS/PCL37	70	10±2
	50	10±2
	30	13±2
	10	20±3
TPS/PCL50	70	2.5±0.4
	50	2.1±0.3
	30	2.9±0.2
	10	5.0±0.8

significant PCL surface enrichment with PCL37, which decreases when screw speed increases.

Both methods lead to the same conclusions, but the values of PCL surface enrichment factor are different. One reason is that surface measurement is approximately 2 μm deep for FTIR and 50 μm for DSC. Higher values of surface enrichment with FTIR suggest that the enrichment is concentrated on a thin layer close to the surface.

Moisture properties

Sorption

The sorption isotherm curves of TPS, PCL and TPS/PCL blends are shown in Fig. 7. As expected, no water absorption is observed for both PCL films. TPS and TPS/PCL blends display similar curve shapes, corresponding to type II of the BET classification [40]. This profile is typically obtained for hydrophilic components, especially for starch based materials

[41, 42]. At low water activities, up to $a_w=0.34$, the plasticizing effect of absorbed water is small, and mobility of polymer chains is limited, water molecules are strongly bound to the polymer. In that case there is no difference between each sample, sorption isotherms are linear, they follow Henry’s law with a constant k_H around 0.09 (calculated from the slope of the linear part of the curves), corresponding to solubility of water in the polymer. For higher water activities, the absorbed water causes a swelling of the polymer and its plasticizing effect increases. Polar groups of starch are then more available for water, so the amount of absorbed water increases more rapidly. Finally some free water molecules appear in the swelling material by aggregation of water molecules on the previous bounded water molecules.

Water content is very similar for TPS and TPS/PCL blends up to $a_w=0.5$. At higher water activities, water content is higher for pure TPS than for TPS/PCL blends.

Water sorption isotherms were fitted according to Park’s model [27]. The results are given in Table 2. The deviation modulus E is below 10 %, indicating that the Park model is consistent with the experimental data and well describes the experimental sorption isotherms.

Langmuir’s terms A_L and b_L have a predominant effect in the low water activity zone ($a_w < 0.1$) [30]. Because of the lack of experimental points for water activity inferior to 0.1, the values obtained for those parameters are not discussed.

The k_H parameter (Henry’s constant) is defined as the random absorption of the water molecules in the materials [29]. The values obtained with Park’s model are consistent with the mean value deduced from the slope of the linear part of the curves (0.09); but they allow distinguishing the behaviour of each sample from the others, with a slight decrease in the adsorption of water molecules for the blends, especially with PCL50.

Fig. 10 Stress–strain curves for PCL, TPS and TPS/PCL blends, stored at 75 % HR

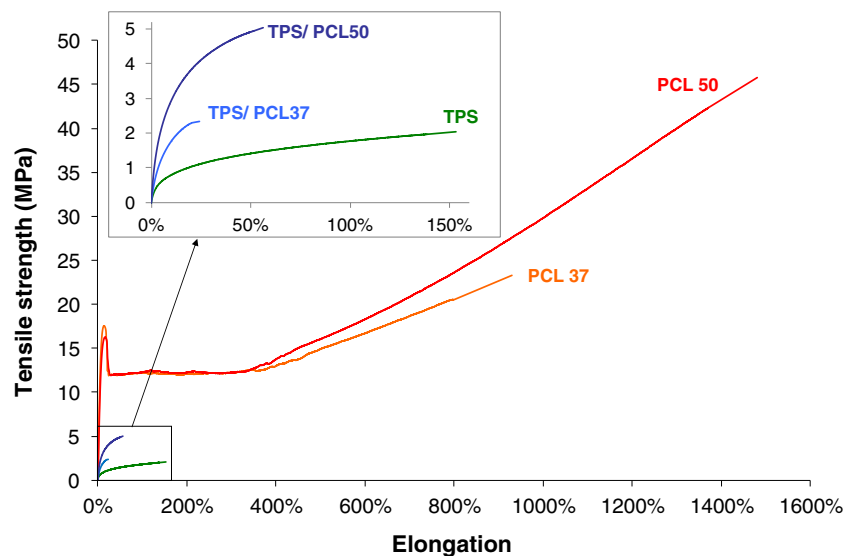


Table 5 Values of mechanical characteristics of TPS, PCL37, PCL50 and TPS/PCL blends (standard deviation)

	Tensile strength (MPa)	Elongation at break (%)
TPS	2.0±0.1	150±9
TPS/PCL37	2.3±0.1	24±2
TPS/PCL50	5.0±0.4	56±5
PCL37	23±3	900±90
PCL50	46±3	1500±90

The equilibrium constant K_a is of the same order of magnitude for TPS/PCL37 and TPS/PCL50; and is lower than for TPS. The mean number of molecules forming an aggregate n_a , is lower for TPS/PCL37 than for TPS; and slightly lower for TPS/PCL50 than for TPS/PCL37. These results traduce a higher ability to form water clusters at high water activities in TPS than in the blends, with a smaller size of the clusters for TPS/PCL50.

Water content was then calculated as the amount of absorbed water related to the starch content in the blend. Corresponding isotherms are presented in Fig. 8. It appears that TPS and TPS/PCL blends display similar behaviours even at low water activities. The slight decrease of water absorption at high water activities previously observed for TPS/PCL blends thus seems to be attributable to the decrease of starch content rather than to a protective effect of PCL, as it was also observed by Myllymäki et al. [15].

Surface properties

Surface tension measurements of TPS, PCL and TPS/PCL films are presented in Table 3. The results are different for the two

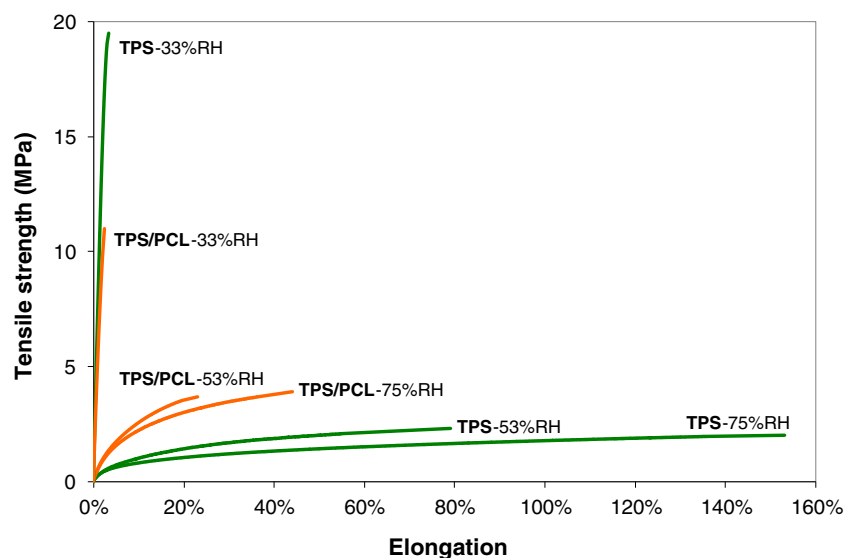
blends; consistently with surface enrichment measurements. A PCL surface enrichment was evidenced for TPS/PCL37; and the surface tension is close to the surface tension of PCL. This confirms the presence of PCL at the surface of this material. On the contrary for TPS/PCL50 no PCL surface enrichment was evidenced and the surface tension is closer to the surface tension of TPS. Nevertheless water contact angle measurements presented below show that the surface of TPS/PCL50 is not free from PCL.

Figure 9 represents the evolution of the relative variation of water contact angle as a function of time for the various samples. The initial angle θ_{max} is given in Table 3. The evolution of contact angle for PCL is due to natural evaporation of water (leading to a water drop of reduced volume on a wet surface); whereas for TPS there is also an obvious spreading and absorption of the drop, due to the hydrophilic nature of the surface of the material.

TPS/PCL blends have very different behaviours. For TPS/PCL50 there is a clear effect of PCL on the surface properties of the blends. The contact angle is closer to pure PCL, which suggests the presence of PCL at the surface of the blend. Since no surface enrichment was observed, PCL50 must be homogeneously distributed in the material and improves water resistance at the surface of the blend.

TPS/PCL37, for which a PCL surface enrichment was evidenced, displays the highest variation of contact angle. To understand this behaviour, surface roughness of the materials was measured (Table 4). Roughness of TPS/PCL37 blends is higher than the other samples, and increases as the screw speed decreases. This heterogeneous surface must be responsible for the lower contact angle.

It was shown above that surface enrichment increases as screw speed decreases for TPS/PCL 37; and no surface

Fig. 11 Stress–strain curves of TPS and TPS/PCL50 at different relative humidities

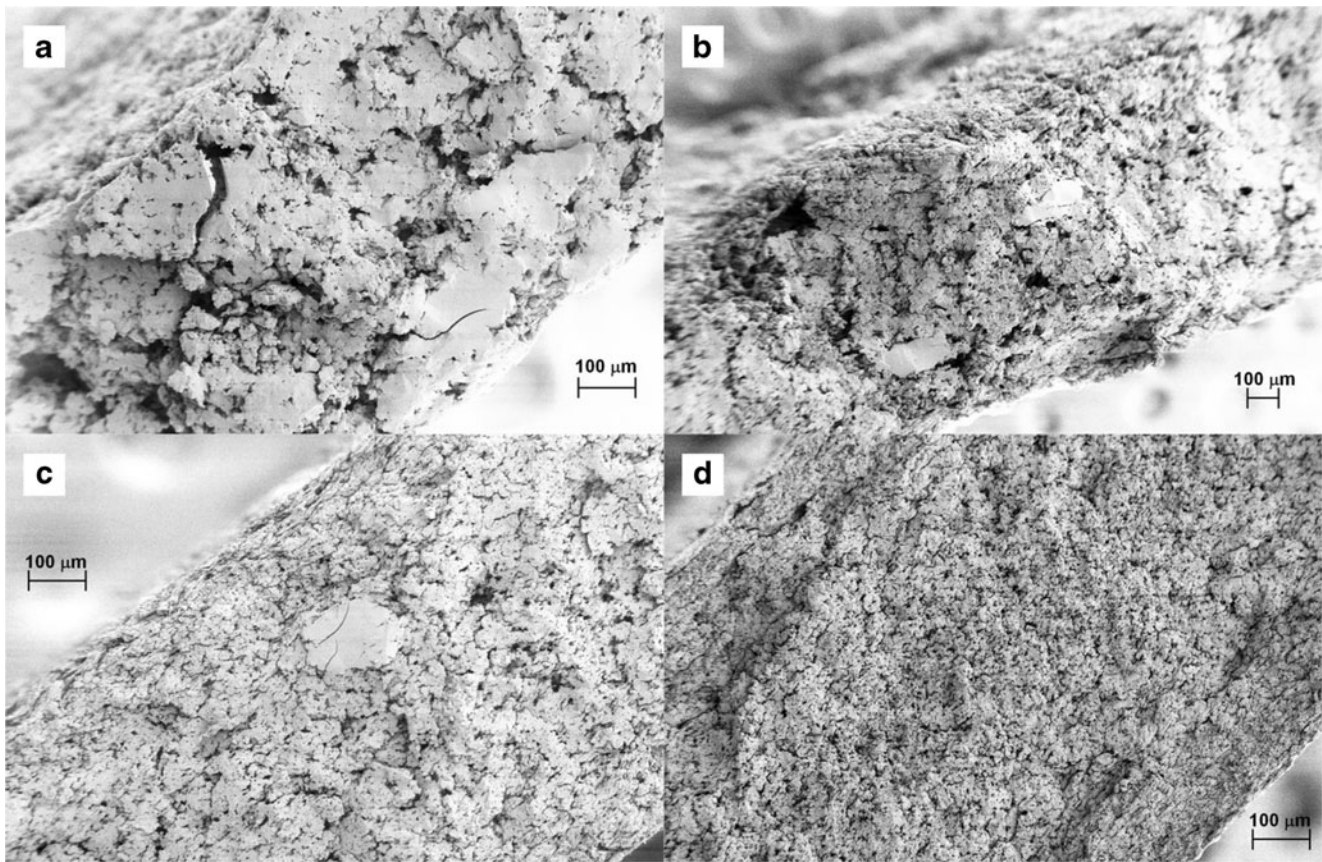


Fig. 12 SEM micrographs of TPS/PCL blends at different screw speeds: TPS/PCL37 processed at 10 rpm (a) and 70 rpm (b) and TPS/PCL50 at 10 rpm (c) and 70 rpm (d)

enrichment was observed with PCL50. Surface roughness measurements clearly indicate that surface enrichment with PCL37 leads to a heterogeneous surface topology. This heterogeneous surface topology may be related to a heterogeneous surface composition, even if surface roughness and heterogeneity in surface composition are two distinct factors

influencing wettability [43]. The surface enrichment is probably not sufficient to obtain a homogeneous PCL layer at the surface. Due to immiscibility between PCL and TPS and different shrinkage factors, the surface may display a topography characterized by a raised surface containing one of the constituent polymers, punctuated by irregular pits containing

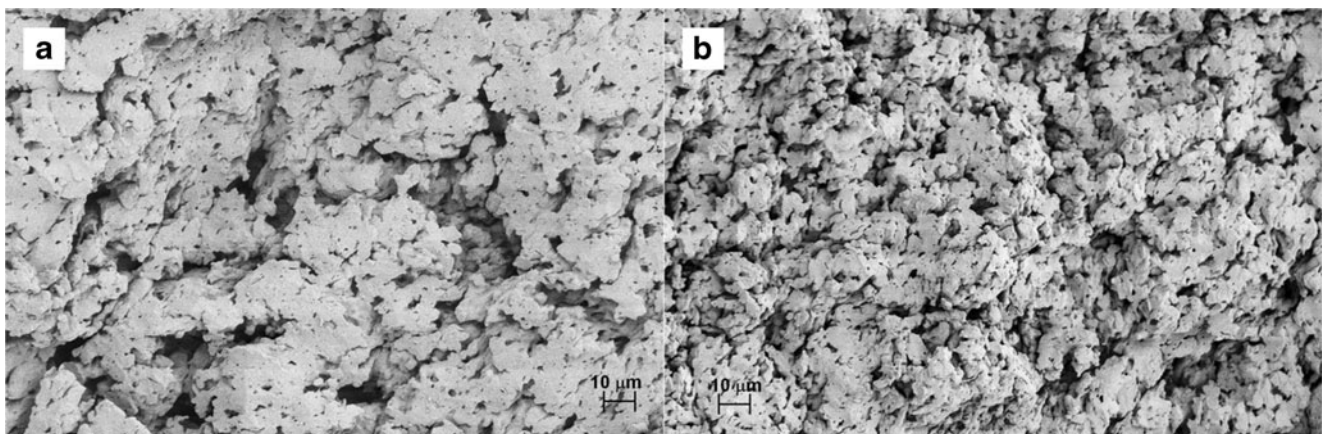


Fig. 13 SEM micrographs of TPS/PCL50 processed at 10 rpm (a) and 70 rpm (b)

the other, as it was already reported for other polymer blends [44]. A more detailed characterization of the surface should be carried out to confirm this assumption.

Finally, PCL surface enrichment does not seem to be the best way of improving surface properties of TPS materials; since surface properties of the blends are closer to PCL properties when no surface enrichment is evidenced.

Mechanical properties

Effects of blending PCL with TPS

Stress–strain curves for different samples are presented in Fig. 10, and the values of stress at break and strain at break are given in Table 5.

Mechanical properties of the blends are closer to pure TPS than pure PCLs. Compared to pure TPS, the tensile strength is higher for the blends and the elongation at break decreases. PCL seems to behave like an incompatible filler dispersed in the TPS matrix. The mechanical properties of TPS/PCL blends may be explained by the incompatibility between the hydrophilic starch and hydrophobic PCL and poor interfacial adhesion between the two components [20, 45].

Besides, DRX analysis has shown that blending with PCL modifies the crystalline structure of starch, which becomes close to less hydrated pure starch. This crystalline effect may contribute to brittleness of the blend materials. Moreover, TPS/PCL50 materials display better mechanical properties than TPS/PCL37. This can be related to the fact that TPS/PCL37 blends are more heterogeneous materials, as suggested by surface enrichment and roughness measurements.

Influence of relative humidity

Mechanical properties were studied at different RH (Fig. 11). For TPS and TPS/PCL blends, tensile strength at break decreases and elongation at break increases as RH increases. This behaviour is known for TPS whose properties are strongly dependent upon humidity [46]. The influence of RH on mechanical properties of TPS/PCL blends seems smaller than for pure TPS, yet the relative variation is similar (e.g. in both cases, elongation is divided by 2 between 75 and 53 % RH). For those samples there is no protective effect of PCL against water; consistently with the conclusion from sorption measurements.

Blends morphology

TPS/PCL blends were studied by Scanning Electron Microscopy after PCL dissolution with dichloromethane (Fig. 12). Dark zones are holes corresponding to extracted PCL, and TPS appears in bright grey. Thermogravimetric measurements indicated that about 2/3 of the initial PCL was removed. Resolution was adjusted to observe the whole edge of the

materials. SEM micrographs are consistent with the observations from surface and mechanical properties: even at higher screw speed, TPS/PCL37 blends appear to be heterogeneous. TPS/PCL50 blends are more homogeneous, all the more at 70 rpm.

Images with higher magnification are given in Fig. 13 for TPS/PCL50 processed at 10 and 70 rpm. They confirm that PCL is more finely dispersed for the blend processed at 70 rpm. The morphology of the blends is thus dependent upon extrusion screw speed, more homogeneous material is obtained at higher screw speeds.

Conclusion

Two TPS/PCL blends were tested, with varying processing conditions. PCL of molecular weight $37\,000\text{ g}\cdot\text{mol}^{-1}$ produces a rough material with a PCL surface enrichment evidenced from DSC and FTIR measurements; whereas with PCL of molecular weight $50\,000\text{ g}\cdot\text{mol}^{-1}$ and a high extrusion screw speed, an homogeneous material is obtained. In both cases the crystalline structure of starch in blends is close to the structure of a less hydrated thermoplastic starch. The affinity of the blends surface for water is reduced in the case of TPS/PCL50 blends; which also displays better mechanical properties than TPS/PCL37 blends. Blending with PCL could be a way of improving TPS resistance to water, at least at the surface of the material; and the best results were obtained with the most homogeneous blends.

Acknowledgments The authors thank the Region Haute Normandie (France) for financial support through its research network VATA (AMI-AMIE project). We also thank the GPM UMR 6634 (University of Rouen) for XRD and SEM experiments.

References

1. Avérous L (2004) *J Macromol Sci C Polym Rev* 44:231–274
2. Hongsheng L, Fengwei X, Long Y, Ling C, Lin L (2009) *Prog Polym Sci* 34:1348–1368
3. Della Valle G, Kozłowski A, Colonna P, Tayeb J (1989) *Lebensm Wiss Technol* 22:279–286
4. Li G, Favis BD (2010) *Macromol Chem Phys* 211:321–333
5. Carvalho AJF (2013) In: Ebnesajjad S (ed) *Handbook of biopolymers and biodegradable plastics*. William Andrew Publishing, Boston
6. Van Tuil R, Fowler P, Lawther M, Weber CJ (2000) In: Weber CJ (ed) *Biobased packaging materials for the food industry: status and perspectives*. KVL, Frederiksberg
7. Dole P, Joly C, Espuche E, Alric I, Gontard N (2004) *Carbohydr Polym* 58:335–343
8. Follain N, Joly C, Dole P, Bliard C (2005) *J Appl Polym Sci* 97:1783–1794
9. Yu L, Dean K, Li L (2006) *Prog Polym Sci* 31:576–602
10. Huneault MA, Li HJ (2012) *Appl Polym Sci* 126:E96–E108
11. Senna MM, El-Shahat HA, El-Naggar AWM (2011) *J Polym Res* 18:763–771

12. Chaléat CM, Halley PJ, Truss RW (2012) *Polym Degrad Stab* 97:1930–1939
13. Yu F, Prashantha K, Soulestin J, Lacrampe MF, Krawczak P (2013) *Carbohydr Polym* 91:253–261
14. Dean K, Yu L, Bateman S, Wu DY (2007) *J Appl Polym Sci* 103:802–811
15. Myllymaki O, Myllarinen P, Forsell P, Suortti T, Lahteenkorva K, Ahvenainen R, Poutanen K (1998) *Packag Technol Sci* 11:265–274
16. Goldberg D (1995) *J Polym Environ* 3:61–67
17. Woodruff MA, Hutmacher DW (2010) *Prog Polym Sci* 35:1217–1256
18. Nien YH, Shih CY, Yang CY, Lu CJ, Ye QX (2013) *J Polym Res* 20:166–171
19. Chiono V, Vozzi G, D'Acunto M, Brinzi S, Domenici C, Vozzi F, Ahluwalia A, Barbani N, Giusti P, Ciardelli G (2009) *Mater Sci Eng C* 29:2174–2187
20. Averous L, Moro L, Dole P, Fringant C (2000) *Polymer* 41:4157–4167
21. Belard L, Dole P, Averous L (2009) *Polym Eng Sci* 49:1177–1186
22. Lee HC (2007) *Physio-chemistry and rheology of Australian lentil flour and starch, and their implications for extrusion*, Ph.D Thesis, University of New South Wales, Sydney, Australia
23. Stevenson DG, Biswas A, Jane JL, Inglett GE (2007) *Carbohydr Polym* 67:21–31
24. Lourdin D, Bizot H, Colonna P (1997) *J Appl Polym Sci* 63:1047–1053
25. Godbillot L, Dole P, Joly C, Rogé B, Mathlouthi M (2006) *Food Chem* 96:380–386
26. Greenspan L (1977) *J Res Natl Bur Stand A Phys Chem* 81A:89–96
27. Park GS (1986) In: Bungay PM, Lonsdale HK, Pinho MN (eds) *Synthetic membranes: science, engineering and applications*. Springer, Netherlands
28. Bessadok A, Langevin D, Gouanvé F, Chappey C, Roudesli S, Marais S (2009) *Carbohydr Polym* 76:74–85
29. Masclaux C, Gouanve F, Espuche E (2010) *J Membr Sci* 363:221–231
30. Alix S, Philippe E, Bessadok A, Lebrun L, Morvan C, Marais S (2009) *Bioresour Technol* 100:4742–4749
31. Owens DK, Wendt RC (1969) *J Appl Polym Sci* 13:1741–1747
32. Leblanc N, Saiah R, Beucher E, Gattin R, Castandet M, Saiter JM (2008) *Carbohydr Polym* 73:548–557
33. Rappenecker G, Zugenmaier P (1981) *Carbohydr Res* 89:11–19
34. Winter WT, Sarko A (1974) *Biopolymers* 13:1447–1460
35. Mercier C, Charbonniere R, Grebaut J, de la Gueriviere JF (1980) *Cereal Chem* 57:4–9
36. Van Soest J, Hulleman S, de Wit D, Vliegthart J (1996) *Ind Crop Prod* 5:11–22
37. Lee K, Knight P, Chung T, Mather P (2008) *Macromolecules* 41:4730–4738
38. Seker M (2004) *Int J Food Sci Technol* 39:1053–1060
39. Wang Y, Rodriguez-Perez MA, Reis RL, Mano JF (2005) *Macromol Mater Eng* 290:792–801
40. Brunauer S, Emmett PH, Teller E (1938) *J Am Chem Soc* 60:309–319
41. Al-Muhtaseb AH, McMinn WAM, Magee TRA (2004) *J Food Eng* 61:297–307
42. Ayadi F, Dole P (2011) *Carbohydr Polym* 84:872–880
43. Chen H, Tang T, Amirfazli A (2012) *Colloids Surf A* 408:17–21
44. Eaton PJ, Graham P, Smith JR, Smart JD, Nevell TG, Tsibouklis J (2000) *Langmuir* 16:7887–7890
45. Shin BY, Lee S, Shin YS, Balakrishnan S, Narayan R (2004) *Polym Eng Sci* 44:1429–1438
46. Chaléat CM, Halley PJ, Truss RW (2008) *Carbohydr Polym* 71:535–543